

Infrared absorption cross-section of SiN_x thin films

Sara N. DiGregorio and Scott D. Habermehl ^{a)}

Sandia National Laboratories, Microelectronics Development Lab, Albuquerque, New Mexico 87185

^{a)} Electronic mail: sdhaber@sandia.gov

At the molecular level, resonant coupling of infrared radiation with oscillations of the electric dipole moment determine the absorption cross-section, σ . The parameter σ relates the bond density to the total integrated absorption. In this work, σ was measured for the Si-N asymmetric stretch mode in SiN_x thin films of varying composition and thickness. Thin films were deposited by low pressure chemical vapor deposition (LPCVD) at 850 °C from mixtures of dichlorosilane and ammonia. σ for each film was determined from Fourier transform infrared spectroscopy and ellipsometric measurements. Increasing the silicon content from 0% to 25% volume fraction amorphous silicon led to increased optical absorption and a corresponding systematic increase in σ from 4.77×10^{-20} cm² to 6.95×10^{-20} cm², which is consistent with literature values.¹ We believe this trend is related to charge transfer induced structural changes in the basal SiN_x tetrahedron as the volume fraction of amorphous silicon increases. Experimental σ values were used to calculate the effective dipole oscillating charge, q , for four films of varying composition. We find that q increases with increasing amorphous silicon content, indicating that compositional factors contribute to modulation of the Si-N dipole moment. Additionally, in the composition range investigated, we found that σ agrees favorably with trends observed in films deposited by plasma enhanced chemical vapor deposition.¹

I. INTRODUCTION

Stoichiometric silicon nitride (SiN_x , $x=1.33$) is a dielectric film widely used in semiconductor applications such as lithographic masking and passivation coatings for surface and bulk defects.²⁻³ Si-rich nitrides ($x < 1.33$) play an important role in microelectromechanical systems (MEMS) due to their chemical and thermal stability as well as their dielectric and elastic properties.⁴⁻⁵ Properties of Si-rich nitrides such as film stress, thermal expansion, elastic modulus, dielectric breakdown, and charge transport have been reported, each revealing strong compositional dependencies.⁶⁻⁹ In general, these dependencies can be accounted for by the Tetrahedron Model for Si-centered, $\text{Si}_y\text{N}_{4-y}$ ($y=0-4$) tetrahedra.¹⁰⁻¹² More recently, Si-rich nitride films have been investigated for reducing propagation losses in integrated nonlinear optics by utilizing SiN_x waveguides that optimize photonic processing of optical signals.¹³ The optical bandgap of silicon nitride allows for high optical intensity buildup with low optical losses and can be tuned with the gas flow ratio in the low pressure chemical vapor deposition (LPCVD) process.¹⁴⁻¹⁵ Fourier transform infrared (FTIR) spectroscopy has been employed to study the vibrational properties of these films, many of which are deposited by LPCVD.

Fundamental molecular vibrations generally occur in the mid-IR spectral region at wavelengths ranging from 2-25 μm ($5000-400\text{ cm}^{-1}$). Resonant coupling between the vibrational modes and incident radiation occurs if the molecular dipole moment is dynamic under vibration.¹⁶ Consequently, the absorption efficiency is substantially determined by the effective dipole charge of the molecule or bond under consideration. In this work FTIR spectroscopy is utilized to interrogate these coupled modes to determine the absorption cross-section, σ , in SiN_x thin films deposited by LPCVD.

The two IR active Si-N modes are the breathing mode centered about 480 cm⁻¹ and the asymmetric stretching mode centered from 830 cm⁻¹ to 875 cm⁻¹.¹⁷⁻¹⁹ In this work the peak location and band area of the asymmetric stretch mode are used to determine σ .

σ is a proportionality factor that relates the bond density to the integrated absorption coefficient.²⁰ For the case of SiN_x films

$$[N] = \frac{1}{\sigma} \int \frac{\alpha(\omega)}{\omega} d\omega \quad (1)$$

where $\sigma = \frac{\pi q^2}{c^2 n \omega_t \mu}$, [N] is the concentration of nitrogen bonds (cm⁻³), ω_t is the peak band

frequency of the vibrational mode (cm⁻¹), q is the effective dipole oscillating charge

(esu), μ is the reduced mass (g), n is the refractive index, c is the speed of light (cm/s),

and $\alpha(\omega)$ is the absorption coefficient (cm⁻¹). $\int \frac{\alpha(\omega)}{\omega} d\omega$ represents the frequency

normalized absorbing oscillator concentration in the film. σ was determined using each

film's unique [N] and experimentally determined absorption coefficient according to Eq.

(1). According to Eq. (1), σ is proportional to the integrated absorption coefficient, and

therefore to the absorption strength.

To achieve accurate results, the absorption coefficient should be determined by transmission and reflection measurements, rather than transmission alone, to account for

reflection effects.²¹ For a thin film deposited on the incident side of a thick substrate, the

transmission is given by the following equation from Brodsky, Cardona and Cuomo

(BCC).²⁰⁻²¹

$$T(\omega) = \frac{(1 - R(\omega))^2 e^{-\alpha_{BCC}(\omega)d}}{1 - R(\omega)^2 e^{-2\alpha_{BCC}(\omega)d}} \quad (2)$$

where $T(\omega)$ is the transmittance, $R(\omega)$ is the reflectance, d is the film thickness, and $\alpha_{BCC}(\omega)$ is the absorption coefficient. Eq. (2) simplifies the full expression for transmittance by assuming reflections at the film/substrate interface are negligible and reflections within the substrate are incoherent.²¹ The absorption coefficient from Eq. (2) is given by²²

$$\alpha_{BCC}(\omega) = \frac{-1}{d} \ln\left(\frac{A(\omega)^2}{T(\omega)} \left[\left(1 + \left(\frac{T(\omega)}{A(\omega)^2 R(\omega)}\right)^2\right)^{1/2} - 1 \right]\right) \quad 3(a)$$

where the function $A(\omega)$ is defined as

$$A(\omega)^2 = \frac{(1 - R(\omega))^2}{2R(\omega)^2}. \quad 3(b)$$

Maley's critique and analysis of the BCC method for determining $\alpha(\omega)$ indicates that for values of the product ωd less than 0.06, the error in $\alpha(\omega)$ increases linearly as ωd approaches zero.²¹ The resulting over-estimation of $\alpha(\omega)$ is primarily a consequence of neglecting multiple internal reflections in the film. In this work ωd varies from 0.01 – 0.05. Applying Maley's formalism yields the thickness-dependent correction

$$\alpha(\omega) = \frac{\alpha(\omega)_{BCC}}{1.26 - 5.3\omega d}. \quad (4)$$

Corrected values for $\alpha(\omega)$ determined by Eqn. (4) are then used to determine the absorption cross-section.

After applying Maley's correction, we do not observe any systematic thickness dependencies in any of the composition ranges investigated. This indicates that the

overall volume of the film does not affect the reported absorption cross-section. The lack of a thickness dependence in the absorption cross-section has been verified as statistically insignificant based on linear regression significance testing.

II. EXPERIMENTAL

The films in this study were prepared in a model 7000 SVG/ Thermco Vertical Thermal Reactor at 850 °C and pressures of 150 to 200 mTorr. Films of varying composition were produced by adjusting the ratio of the dichlorosilane (SiCl_2H_2) flow to the total flow ($\text{SiCl}_2\text{H}_2 + \text{ammonia (NH}_3)$) in the reactor from 0.23 to 0.92. The substrates used in this study were p-type Si(100) with a resistivity of 2-20 ohms and either 150mm or 200mm in diameter.

The thickness and composition for each film was determined from ellipsometric data using the Bruggemann Effect Medium Approximation (BEMA).²³ The films were modeled as a combination of Si_3N_4 and a-Si, with an assumption of zero void density. Measurements were performed on a dual wavelength Rudolph S2000 ellipsometer at 633 and 780 nm. The composition ranged from 0-25% volume fraction amorphous silicon (V_{Si}). The thickness ranged from 136-558 nm. The densities of the films were determined by mass and thickness measurements.²⁴ The nitrogen concentration [N] of each film was determined from V_{Si} and density measurements.²⁴

T and R were collected for each film using a Thermo Scientific iS50 FTIR spectrometer in the spectral range of 400-4000 cm^{-1} , with a resolution of 4 cm^{-1} . The samples collected exhibited no evidence of Si-H or N-H bonding, as detected to within

the 1 at% sensitivity of the spectrometer. This is primarily a consequence of the high deposition temperature which renders H-bonding energetically unfavorable.

The error associated with the reported σ values considered the measurement uncertainty, the propagated error, and the error associated with baseline correction. The average error in the experiments was 2-3%.²⁴ Comparable studies report an error of less than 10%.²¹

There are numerous references to the formation of Si nanocrystals in SiN_x thin films.^{18,25} High resolution transmission electron microscopy images of comparable films to those in this study exhibit no evidence of Si nanocrystal formation, which is consistent with results for films with $x > 1$.²⁵

III. RESULTS AND DISCUSSION

Figure 1 displays $T(\omega)$ and $R(\omega)$ for a representative film that is 472.9 nm thick with $V_{\text{Si}}=3.7\%$ a-Si. The Si-N asymmetric stretching band is observed at 850.5 cm^{-1} and the Si-N breathing mode is seen at 472 cm^{-1} .

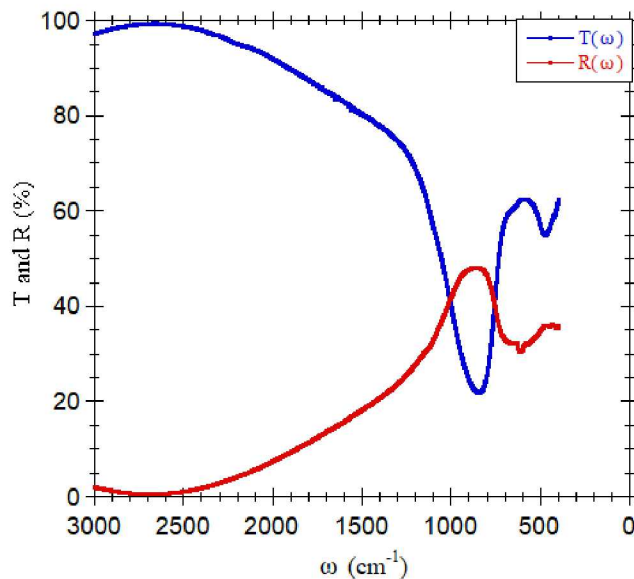


FIG. 1. Transmission and reflection spectra for a SiN_x film 472.9 nm thick and 3.7% a-Si.

Using Eq. (2) combined with T and R data, the absorption coefficient, $\alpha_{\text{BCC}}(\omega)$ was determined for each film. Figure 2 displays the $\alpha_{\text{BCC}}(\omega)$ curves for four films in the 226.6-289.2 thickness range with varying compositions.

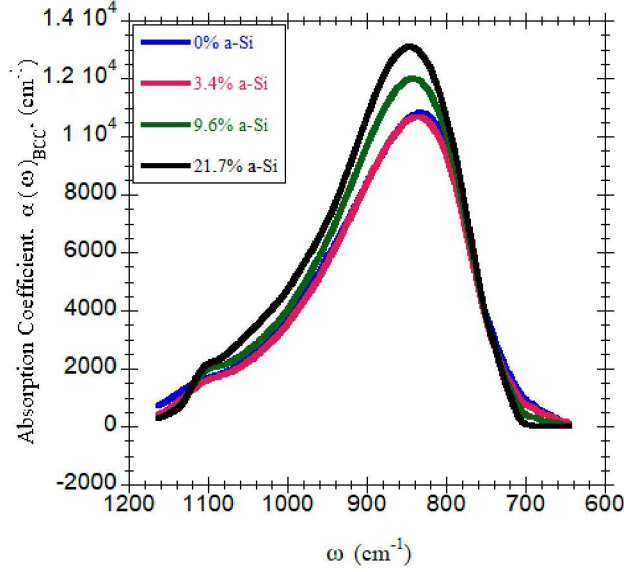


FIG. 2. Absorption coefficient $\alpha(\omega)_{\text{BCC}}$ for SiN_x films in the 226.6-289.2 nm thickness range with varying compositions.

Figure 2 demonstrates that the integrated absorption coefficient and ω_t increase monotonically with V_{Si} . An increase in the magnitude of the absorption coefficient corresponds to a higher absorption probability. From the trend in Figure 2, we conclude that the absorption probability increases as the films become more Si-rich.

Figure 2 also shows that ω_t shifts to higher frequencies as V_{Si} increases. This trend is generally true for all thickness ranges as listed in Table I. According to the central force model, bond strain is correlated to frequency shifts in the Si-N vibrational mode and can be estimated by Eq. (5)^{10,26-28}

$$\varepsilon = \frac{V_1 - V_2}{V_1} \quad (5)$$

where ε is the film strain, v_1 is associated with a zero-strain condition (taken here-in to be 848 cm^{-1}) and v_2 is ω_t .²⁶ The observed increase in ω_t with increasing V_{Si} indicates that an increase in V_{Si} is associated with less tensile film strain. This result is explained by the relationship between V_{Si} and compositionally-induced volumetric distortion in the $\text{Si}_y\text{N}_{4-y}$ ($y= 0-4$) tetrahedral unit.⁷

For each film, σ was determined from Eq. (1) where σ is equal to $\int \frac{\alpha(\omega)}{\omega} d\omega / [\text{N}]$. $[\text{N}]$ for each film ranged between 3.98×10^{22} and 5.29×10^{22} molecules/ cm^3 .

The associated relationships between σ and its determining parameters are listed in Table I.

TABLE I. The film composition, $[\text{N}]/[\text{Si}]$, amorphous silicon volume fraction, V_{Si} , thickness, d , peak frequency of the Si-N asymmetric stretch mode, ω_t , and absorption cross-section, σ , for each film.

$[\text{N}]/[\text{Si}]$	V_{Si} (% a-Si/100)	d (nm)	ω_t (cm^{-1})	σ ($\times 10^{-20} \text{ cm}^2$)
1.33	0	142.7	831.2	5.06 \pm .12
1.33	0	143.6	830.2	5.11 \pm .12
1.33	0	236.5	834.1	4.97 \pm .13
1.33	0	238.2	835.0	5.02 \pm .12
1.32	.010	468.3	842.8	4.96 \pm .12
1.32	.011	471.8	845.7	4.77 \pm .12
1.28	.033	143.1	834.1	5.37 \pm .15
1.28	.033	150.3	831.7	5.33 \pm .15
1.28	.034	264	837.5	4.94 \pm .15
1.27	.039	276.3	839.0	4.97 \pm .11
1.27	.037	472.9	850.5	5.06 \pm .15
1.28	.036	498	845.7	5.27 \pm .17
1.29	.026	557.9	849.5	5.51 \pm .15
1.19	.092	150.6	835.5	6.16 \pm .09
1.18	.102	154.3	838.9	6.25 \pm .09
1.17	.107	288.2	842.3	5.78 \pm .10

1.18	.096	289.2	842.3	5.72±.15
1.18	.097	493.8	850.0	6.23±.14
1.17	.106	507.5	853.9	5.85±.11
0.98	.231	136.2	842.8	6.85±.15
0.96	.245	161	841.8	6.75±.15
1.00	.217	226.6	842.8	6.89±.24
0.96	.250	265.3	846.1	6.95±.22
0.98	.234	445.2	853.4	6.52±.15
0.96	.244	531.2	857.7	6.63±.17

The data in Table I that is plotted in Figure 3 demonstrates that in the range of V_{Si} from 0-25% a-Si we observe a systematic increase of σ from $4.77 \times 10^{-20} \text{ cm}^2$ to $6.95 \times 10^{-20} \text{ cm}^2$. This trend supports the previous discussion of Figure 2, which established that increasing V_{Si} results in higher absorption probabilities. This dependence has been verified as statistically significant on the basis of linear regression significance testing.

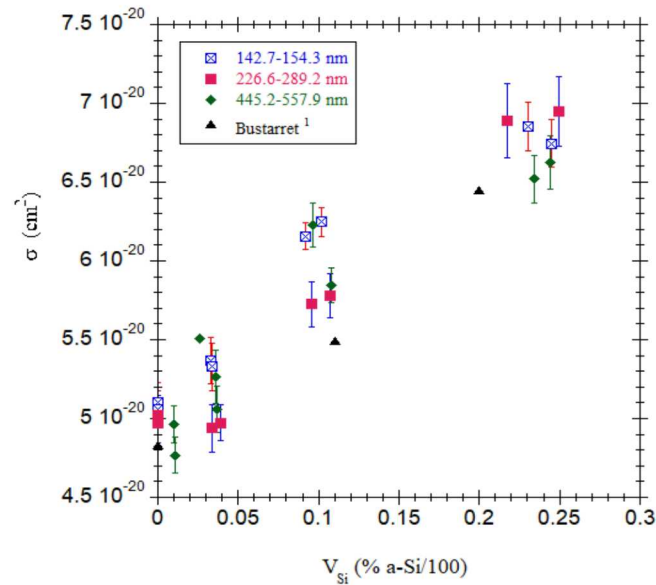


FIG. 3. Absorption cross-section, σ , for SiN_x films of varying composition and thickness, from this work and ref [1].

According to Eq. (1), σ is fundamentally dependent on $[N]$ and the absorption coefficient, which are both affected with increasing V_{Si} . An increase in V_{Si} is associated

with structural changes that correspond to the absorption strength of the Si-N dipole moment. In the previous discussion of Figure 2 we have also shown that an increase of V_{Si} forces the local bonding structure to shift, thus, we conclude that less tensile films experience higher absorption probabilities and therefore greater absorption cross-sections.

This result is believed to be related to changes in Si-Si_yN_{4-y} tetrahedral structure as the more electronegative N atom is substituted for a less electronegative Si atom.¹⁰ The argument underlying the tetrahedron model is that the partially ionic nature of the Si-N bond induces a charge transfer as substitution of one or more Si atoms for an electronegative N atom modifies the charge distribution of the adjacent bonds.¹⁰ The modified charge distribution is believed to affect the Si-N bond absorption effectiveness, and therefore σ , as the composition changes.

The trends observed in the LPCVD films of this study are nearly identical to those for films deposited by plasma enhanced chemical vapor deposition (PECVD) reported by Bustarret, et al.¹ The consistency between the literature and our experimental σ results are displayed in Figure 3 at V_{Si} values of 0, 11, and 20% a-Si. The agreement between the two trends infers that impurities introduced by PECVD processes do not appreciably affect the Si-N bond charge distribution.

The parameter q , known as the effective dipole oscillating charge²⁹, determines the coupling strength between molecular vibrations and incident radiation; it is a critical factor when determining σ . Using Eq. (1), we calculated q for four representative films from Table I; two films for 0 and 10% a-Si each. q was calculated using our experimentally determined values for ω_i and σ , combined with index of refraction data

obtained from IR ellipsometry.²⁴ In determining q , it was assumed that compositionally induced changes in the effective mass of the Si-N system were negligible. Table II lists the q values for each of the four films, along with the parameters used in determining them.

TABLE II. Amorphous silicon volume fraction, V_{Si} , peak frequency of the Si-N asymmetric stretch mode, ω_t , index of refraction, n , experimentally determined absorption cross-section, σ , and effective dipole oscillating charge, q , electrostatic units (esu).

V_{Si} (% a-Si/100)	ω_t (cm^{-1})	n	σ ($\times 10^{-20} \text{ cm}^2$)	q (esu)
0	831.2	3.201	5.06	1.62e
0	830.2	3.22	5.11	1.63e
.097	850.0	3.03	6.23	1.76e
.106	853.9	2.94	5.85	1.69e

In the range of V_{Si} from 0-10% a-Si we find that q increases from a range of 1.62e-1.63e to 1.69e-1.76e, where e is the elementary charge.²⁹ In previous studies it was reported that q typically ranges between .3e and 3e.²⁹ Our results are commensurate with this expected magnitude of q . Figures 2 and 3 demonstrate that the strain and absorption-cross section share the same relationship with increasing V_{Si} . This suggests that the coupling strength of the Si-N bond is related to strain changes in the Si-Si_yN_{4-y} tetrahedral unit where q increases in films that are more Si-rich. Si-rich films exhibit a higher degree

of isolated Si-N bonds which implies that the coupling strength and IR absorption are enhanced by Si-N bond isolation.

IV. SUMMARY AND CONCLUSIONS

The IR absorption cross-section, σ , for LPCVD SiN_x films of composition ranging from V_{Si}= 0-25% a-Si and thickness ranging from 136-588 nm were measured. We find that σ increases from 4.77×10^{-20} cm² to 6.95×10^{-20} cm² with increasing V_{Si}. This result is believed to be related to compositionally induced changes in the Si-N bond charge distribution resulting from the substitution of less electronegative Si for N in the amorphous network and, more fundamentally, the concomitant increase in the effective dipole oscillating charge parameter, q . Higher σ values associated with increases in V_{Si} imply that isolated Si-N bonds have a higher coupling strength and therefore a greater IR absorption efficiency.

V. ACKNOWLEDGMENTS

We thank the Sandia MESA SiFab process group for assistance with SiN_x film preparation and general process support. We gratefully acknowledge J. Ginn for the IR ellipsometry data, and M. Berg and A. Leenheer for insightful discussions.

Sandia National Laboratories is a multimission laboratory managed and operated by National Technology & Engineering Solutions of Sandia LLC, a wholly owned subsidiary of Honeywell International Inc., for the U.S. Department of Energy's National Nuclear Security Administration under contract DE-NA0003525.

This paper describes objective technical results and analysis. Any subjective views or opinions that might be expressed in the paper do not necessarily represent the views of the U.S. Department of Energy or the United States Government.

VI. References

1. E. Bustarret, M. Bensouda, M. Habrard, and J. Bruyere, *Phys. Rev. B* **38**, 8171 (1988).
2. H. Sato, A. Izumi, and H. Matsumura, *Appl. Phys. Lett.* **77**, 2752 (2000).
3. W. Lanford and M. Rand, *J. Appl. Phys.* **49**, 2473 (1978).
4. B.C. Joshi, D.P. Runthala, B.B. Dixit, O.P. Wadhawan, and P.D. Vyas, *Indian Journal of Engineering and Material Sciences* **7**, 303 (2000).
5. P. Jhang, C. Lu, J. Shieh, L. Yang, T. Yang, and K. Chen, *Solid State Electronics* **133**, 10 (2017).
6. S. Habermehl, *J. Vac. Sci. Technol. A* **36**, 021517 (2018).
7. S. Habermehl, *J. Appl. Phys.* **83**, (1998).
8. S. Habermehl, R.T. Apadaca, and R.J. Kaplar, *Appl. Phys. Lett.* **94**, 012905 (2009).
9. S. Habermehl, and R.T. Apadaca, *Appl. Phys. Lett.* **84**, (2003).
10. S.J. Gurman, *J. Non-cryst. Solids* **143**, 207 (1992).
11. D.E. Aspnes and J.B. Theeten *J. Appl. Phys.* **50**, 4929 (1979).
12. H.R. Philipp, *J. Electrochem. Soc.* **120** 295 (1973).
13. M. Dizaji, J. Kruckel, A. Fulop, P. Andrekson, V. Torres-Company and L. Chen *Optics Express* **25** 12100 (2017).
14. J. Kruckel et al, *Optics Express* **25** 15370 (2017).
15. J. Kruckel et al, *Optics Express* **23** (2015).
16. D.C. Harris and M.D. Bertolucci, *Symmetry and Spectroscopy* (Oxford University Press, NY, 1978).
17. Z. Yin, and F.W. Smith, *Phys. Rev. B* **42**, (1990).
18. G. Scardera, T. Puzzer, G. Conibeer, and M.A. Green, *J. Appl. Phys.* **104**, 104310 (2008).
19. G. Lucovsky, J. Yang, S.S. Chao, J.E. Tyler, and W. Czubaty, *Phys. Rev. B* **28**, 3234 (1983).
20. M.H. Brodsky, M. Cardona, and J.J. Cuomo, *Phys. Rev. B* **16**, 3556 (1977).
21. N. Maley, *Phys. Rev. B* **46** (1992).
22. B. Pajot, *Analisis* **7**, 293 (1977).
23. D.A.G. Bruggeman, *Ann. Phys. (Leipzig)* **24**, 636 (1935).
24. See supplementary material at [URL will be inserted by AIP publishing] for a more thorough account of procedural details.
25. L.E. Hintzsche, C.M. Fang, T. Watts, M. Marsman, G. Jordan, W.P.E. Lamers, A.W. Weeber and G. Kresse, *Phys. Rev. B* **86**, (2012)
26. P.N. Sen and M.F. Thorpe, *Phys. Rev. B* **15**, 4030 (1977).
27. J.T. Fitch, G. Lucovsky, E. Kobeda, and E.A. Irene, *J. Vac. Sci. Technol. B* **7**, 153 (1989).
28. M.D. Newton and G.V. Gibbs, *Phys. Chem. Miner.* **6**, 221 (1980).
29. M. Stavola, and W.B. Fowler, *J. Appl Phys.* **123**, 161561 (2018).
30. A. Clifford, *Multivariate Error Analysis*. (1973).
31. K.E. Atkinson, *An introduction to Numerical Analysis* (2nd ed), (1989).